A three-dimensional Vp, Vs, and Vp/Vs crustal structure in Fujian, Southeast China, from active- and passive-source experiments

Hui-Teng Cai [a,b], Hao Kuo-Chen [c,*], Xin Jin [a,b], Chien-Ying Wang [c], Bor-Shouh Huang [d], Horng-Yuan Yen [c]

[a] College of Civil Engineering, Fuzhou University, Fuzhou, China
[b] Earthquake Administration of Fujian Province, Fuzhou, China
[c] Department of Earth Sciences, National Central University, Jhongli, Taiwan
[d] Institute of Earth Sciences, Academia Sinica, Taipei, Taiwan

A B S T R A C T

Fujian, Southeastern China, has experienced multistage tectonic activities since the Neoproterozoic Era and is currently influenced by collision between the Eurasian and Philippine Sea plates. Topography, fault zones, and patterns of seismicity are the imprints of tectonic evolution. Historically, there have been several catastrophic earthquakes in the southeastern part of Fujian. To understand the crustal structure related to the fault zones, we performed Vp, Vs, and Vp/Vs travel-time tomography using joint inversion of active and passive sources. A total of 75,827 and 31,044 arrivals of P and S waves, respectively, from 33 explosions and 2543 earthquakes are used in our study. As a result, seismicity has indicated that two NE strike seismogenic zones, the Zhenghe–Dapu and Changle–Zhaoan fault zones, are currently active. Low Vp/Vs ratios in inland Fujian imply that the crust is mainly composed of felsic rocks as part of the Eurasian continental crust, which is consistent with geological observations at the surface. Based on Vp tomography, the thickness of the crust along the coastline is shallower than that on land, which is related to higher heat flow and the Bouguer anomaly. This shallow crust phenomenon near the coastline could be related to the regional extensional stress: the remaining structure of the back-arc extension that stretched the continental crust during the Mesozoic Era or/and the Cenozoic extension due to South China sea opening in Taiwan Strait.

1. Introduction

Fujian is located at the southeastern continental margin of the Eurasian plate (EUP), which strongly interacts with the Philippine Sea plate (PHSP) near the Taiwan orogen (Fig. 1a). The continental margin of Southeast China has developed into a series of fault basins that features fault bays and plains in coastal areas. The NNE-NE trend of the Zhenghe–Dapu fault zone is the tectonic boundary, an ancient suture zone, that separates the Early Paleozoic fold belt to the west from the Late Mesozoic magmatic belt to the east (Jahn et al., 1976; Fujian, 1985; Chen et al., 2002; Shu et al., 2011). The fault and fault-depression basins of the Late Cretaceous-Paleogene primarily lie on the western side from the Yanshanian tectonic period (175–135 Ma), and most of these basins were extinct by the Quaternary Period; the fault basin and

bay were well developed on the eastern side in the Quaternary (Ding et al., 1999; Wan, 2012).

Three major NNE-NE-oriented faults exist, the Changle–Zhaoan fault zone (Fault A of Fig. 1b), the Zhenghe–Dapu fault zone (Fault B of Fig. 1b), and the Shaowu–Heyuan fault zone (Fault C of Fig. 1b), whose structures are well developed and often exhibit large-scale long extension, a cutting crust, and multistage activities since the Early Paleozoic Era (Fig. 1b) (e.g., Shu et al., 2011; Wan, 2012). However, there are several NNW-NW-oriented fault zones perpendicular to the NNE-NE main fault zones (Fig. 1b). Thus, these faults constitute the basic tectonic framework of the continental margin of Southeast China. Geophysical observations at the surface have implied that the crustal structure from the coastline to inland Fujian (from east to west) changes dramatically. In terms of the Bouguer anomaly (BA), the values are higher along the coastline than those of inland Fujian, and the differences between these two areas can be up to 70 mgal (Fig. 1c) (Fujian, 1992). Moreover, heat flow patterns also show considerable contrast between the coastline and inland Fujian: higher values along the
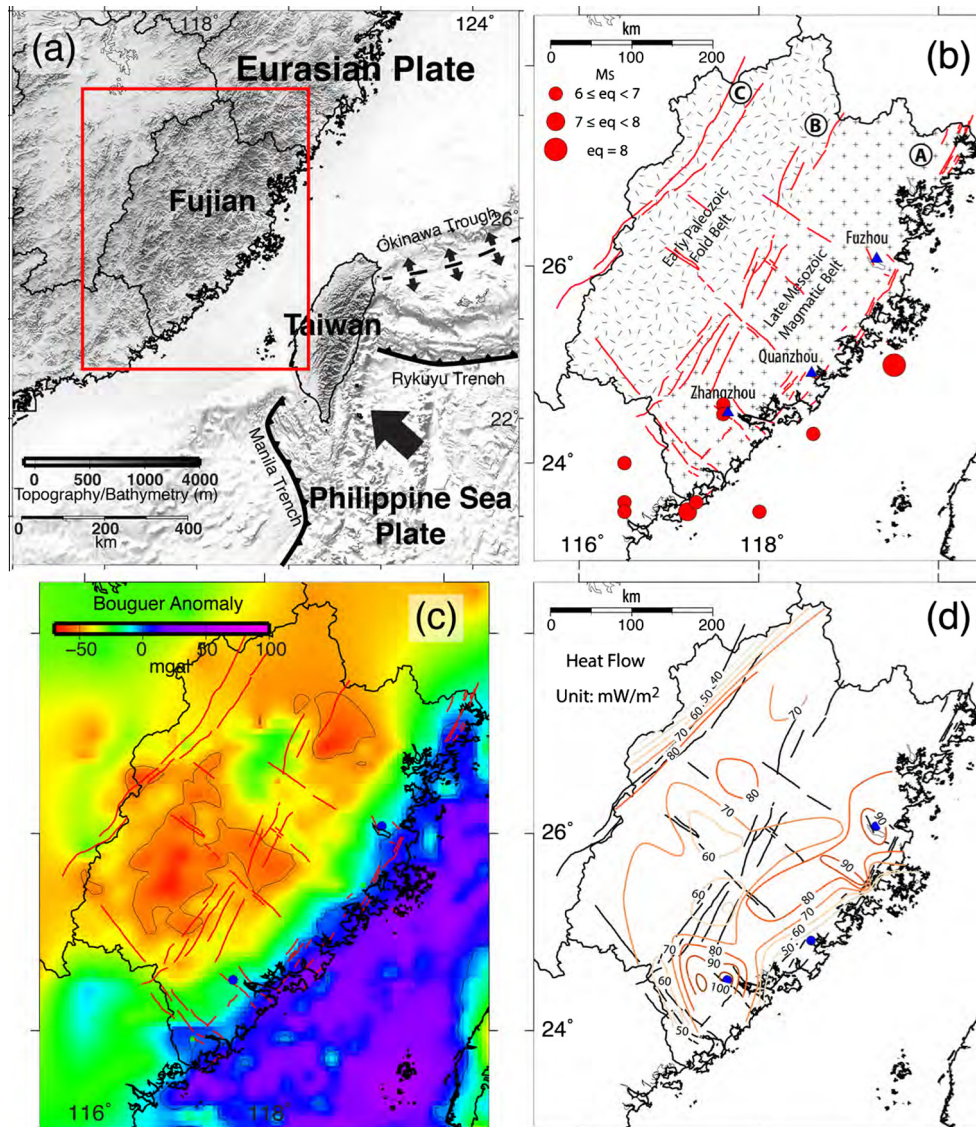
Fig. 1. Tectonic setting, Bouguer anomaly, and heat flow in Fujian. (a) Tectonic setting of southeastern China. Red rectangular area: study region. Black arrow: motion of the Philippine Sea plate (Yu et al., 1997). (b) Tectonic setting of Fujian and locations of large earthquakes (Ms> 6) (Ding et al., 1999). Blue triangle: major city. Red circle: earthquake. Red line: fault zone (A: Changle–Zhaoan fault zone; B: Zhenghe–Dapu fault; C: Shaowu–Heyuan fault zone). (c) Bouguer anomaly (Fujian, 1992). (d) Heat flow (Fujian, 1992). (For interpretation of the references to color in this figure legend, the reader is referred to the web version of this article.)

coastline and lower values for inland Fujian (Fig. 1d) (Fujian, 1992; Ding et al., 1999; Hu et al., 2000).

Several major earthquakes (Ms ⩾ 6) have been recorded across the coastline near the cities of Quanzhou and Zhangzhou since 1067 (Fig. 1b). Most moderate earthquakes (Ms. 5–6) were distributed around these two cities, and seismic activity weakened in the inland direction (Ding et al., 1999). In 1604, an earthquake with Ms. 8.0 occurred in the eastern offshore of Quanzhou that was the largest one recorded in this region and caused many landslides and collapsed buildings. Based on historical ground shaking and the distribution of aftershocks, the rupture plane of this earthquake is 38° N strike with 54° dipping to the east, and the principal compression axis is 80°, which is related to the NW direction movement of the Philippine Sea plate (Fig. 1a) (Ding et al., 1999). In 1067, 1185 and 1445, there were three large earthquakes (Ms > 6) near Zhangzhou on land, potentially implying the high seismic hazard risk in this region due to large population

(∼340,000 residents) in the city (Ding et al., 1999). However, the fault planes of those earthquakes are still disputed owing to the earthquake locations near the junction between the NE and NW fault zones (Fig. 1b).

Fujian has experienced multiple tectonic events since the Paleozoic Era that have formed the current crustal structure. At the surface, the geological provinces have been mapped (e.g., Jahn et al., 1976; Chen et al., 2002; Wang and Shu, 2012). However, the detailed crustal structure of Fujian has not been studied thoroughly, which is important for understanding the major fault zones related to the crustal structure. Seismic tomography is a useful tool for imaging the subsurface. Thus, to obtain the fine-scale crustal structure, we performed a joint inversion of both active (explosion) and passive (earthquake) sources. We designed active-source experiments from 2008 to 2012 to constrain the upper crustal structure, and passive sources from 2001 to 2014 recorded in the permanent seismic network of the Earthquake

Administration of Fujian Province are also included to constrain the middle to lower crust in our tomography. In previous studies, those seismic images were only resolved for the upper mantle structure due to the use of teleseismic events (Huang and Zhao, 2006; Huang et al., 2010; Zheng et al., 2013). Hence, we used explosions and local earthquakes to complete the record for seismic images of the crust from previous studies. In this study, we present the first detailed 3D crustal Vp, Vs, and Vp/Vs tomography in this region and discuss heat flow, the Bouguer anomaly, and earthquakes related to the crustal structure in Fujian.

2. Data and analysis

The seismograms used in this study were recorded both by seismic stations operated as part of the TAIGER (Taiwan Integrated Geodynamic Research) (Wu et al., 2014) and ATSEE (Across Taiwan-Strait Explosion Experiment) projects and by permanent

seismographs on the Earthquake Administration of Fujian Province (EAFP) (Fig. 2a and b). To obtain the fine-scale upper crustal structure in Fujian and Taiwan, 33 shots were executed on land and recorded by 5797 seismic stations onshore and offshore, with 48,895 P wave arrivals from 2008 through 2013 by TAIGER, ATSEE, and EAFP (Fig. 2b and d). Examples of the waveforms and arrivals picks with dense arrays are shown in Fig. 3. The structure of the middle to lower crust can be constrained by the ray paths between earthquakes and seismic stations. A total of 3203 earthquakes recorded in 97 broadband seismic stations of EAFP from 2001 to 2014 from EAFP event catalogue (Fig. 2a and c) and the magnitude of events range from 0.5 to 4.8. However, in order to obtain a good constraint on determining earthquake locations, we only use 2543 events with at least 10 arrivals (including at least one S wave arrival). In total, there were 75,827 and 31,044 arrivals of P and S waves, respectively, from explosions and earthquakes for tomography inversion (Fig. 4). The data quality of the arrivals can be shown in terms of the figure
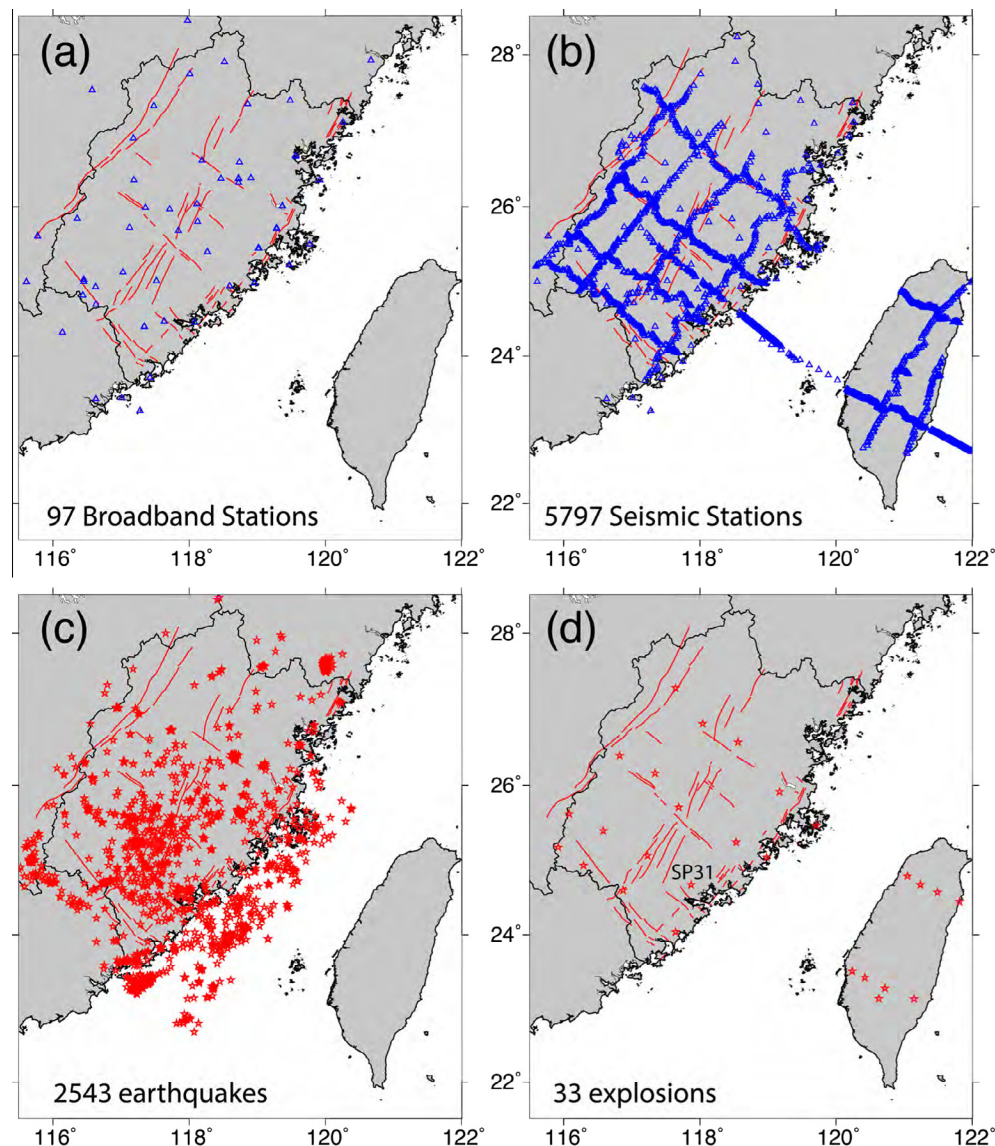

Fig. 2. Seismic station networks and active and passive sources. (a) Broadband seismic network in Fujian. (b) Temporary seismic network for recording active sources. (c) Distribution of earthquakes used in this study. (d) Distribution of explosions.
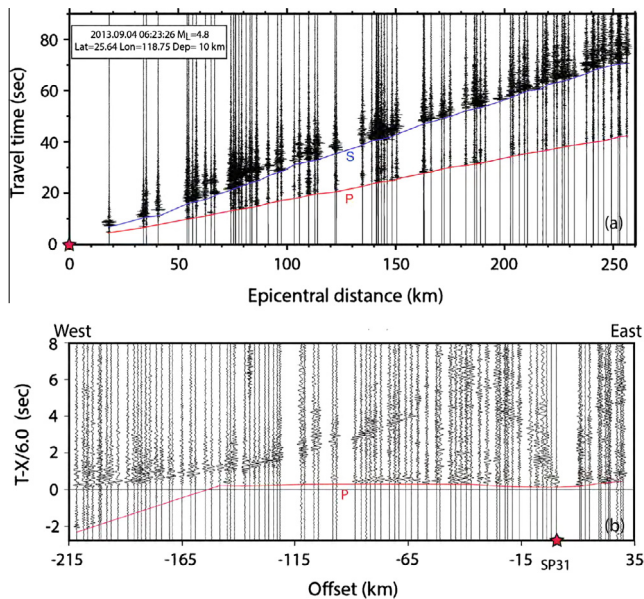
Fig. 3. Examples of seismic waveforms and arrival picks from (a) an earthquake and (b) an explosion. See Fig. 2d for explosion SP31 location.

Table 1
Seismometers used in this study.

Experiment	Seismometer	Frequency range
Passive source	CMG-3ESPC-60	60 s–50 Hz
	CMG-3ESPC-120	120 s–50 Hz
	CTS-1	120 s–50 Hz
	BBVS-60	60 s–50 Hz
	FSS-3B	2 s–50 Hz
	FSS-3M	2 s–50 Hz
Active source	PDS-1	30 s–80 Hz
	I4-C OBS	60 s–50 Hz

P-velocities. Local earthquake hypocenters are adjusted at each iteration, whereas shot locations remain fixed.

Considering the distribution of receivers and sources, we used a 18 × 18 km spaced grid in the horizontal that allowed for adequate spatial resolution for crustal features. This model was 800 km long in both horizontal directions and 93 km in depth. We used non-uniform grids in depth to allow finer resolution where station density is relatively high. In the vertical direction, the grid intervals varied from 3 km in the top 15–6 km for depths of 15–93 km. The starting model was the 1D model determined by Cai et al. (2015) for the Fujian region.

of travel times versus hypocentral distances of shots and earthquakes (Fig. 4b). Table 1 has summarized the seismic instruments we used in both passive- and active-source experiments.

We analyzed our arrival time data using the finite difference arrival time tomography algorithm described in Roecker et al. (2004, 2006) to obtain 3D velocity structures. Our region of interest (800 × 800 km) is too large to be treated accurately as a flat Earth; thus, to avoid the biases introduced by either inserting a spherical Earth in a Cartesian system or applying Earth-flattening transforms to a laterally heterogeneous model, we computed travel times by adapting an Eikonal equation solver based on that of Vidale (1988) and Hole and Zelt (1995) directly to a spherical coordinate system. The arrival time tomographic inversion involves two principal steps. The first locates local earthquakes in an existing model through an interpolated grid search. The second calculates ray paths from all sources to recording stations and forms a system of linear equations that are then solved for perturbations to

3. Resolution test

The travel time residuals from the 1D model to the 3D preferred final model were significantly reduced after 6 iterations and both P and S wave residuals of 3D preferred final model are near normal distributions (Fig. 5). The ray coverage and numbers of ray hits in grid points with different depths are shown in Fig. 6. The numbers of ray hits are on the order of hundreds down to 39 km depth for both P and S waves. Benefiting from the uniform distribution between active sources and earthquakes and stations, most regions in Fujian are well covered in terms of rays passing through; for example, at depths of 6–39 km, all but one transect with over 1000 ray counts from Fujian to Taiwan (Fig. 6). To test the resolution of the 3D model, we preformed the checkerboard test; the anomalies of the block sizes were 72 × 72 km^2 in the horizontal and 15 km in depth, and the perturbation of the model was ±10% (Fig. 7). As a result, the resolution of the 3D model can be as low
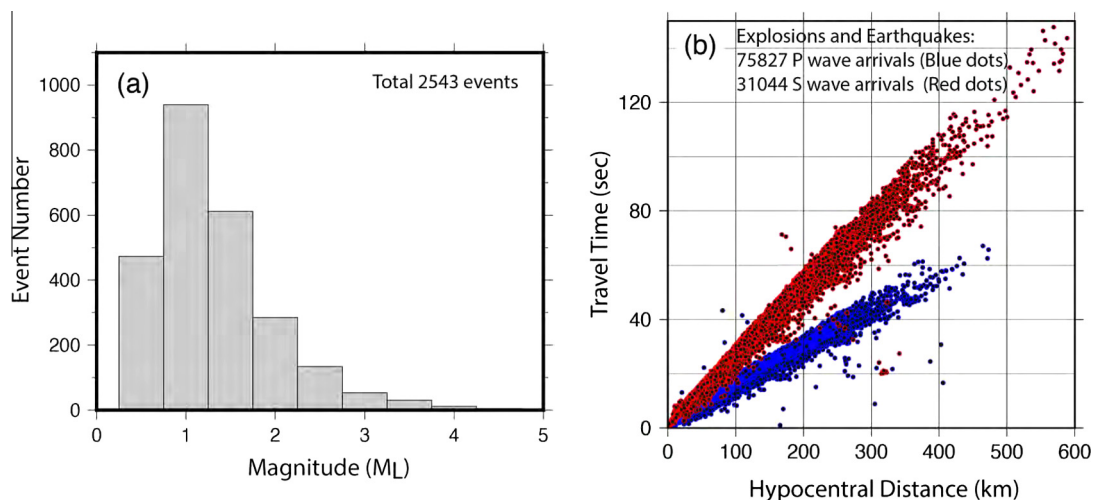

Fig. 4. Magnitude distribution of the earthquakes used in this study and travel times versus hypocentral distance of arrivals. (a) Magnitude distribution of the earthquakes. (b) P and S wave arrivals from explosions and earthquakes.
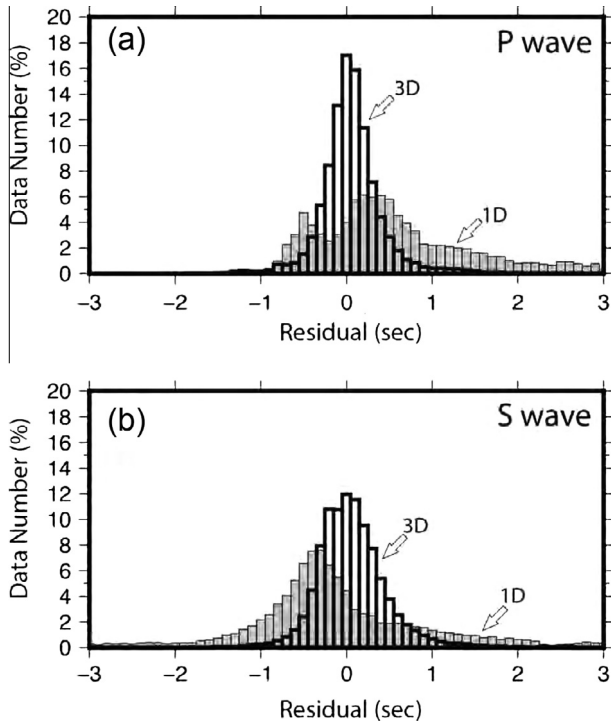
Fig. 5. Travel time residuals from 1D velocity model and 3D model. (a) Travel time residuals of P wave. (b) Travel time residuals of S wave. Gray column: 1D velocity model. Thick line column: 3D velocity model.

as 39 km for both P and S waves in most of the Fujian region. Notably, even with one transect having extremely high ray hits, as mentioned above, the result of the checkerboard test was not affected by this factor (Fig. 7), indicating uniform velocity perturbations at different depths.

4. Results

Fig. 8 shows map views of Vp, Vs, and Vp/Vs ratios at different depths. At depths of 0 and 6 km, Vp in Fujian are higher than those in the sedimentary basin of the Coastal Plain of Taiwan but are similar to those in the mountain belt of Taiwan. The patterns of Vp are related to the NE and NE fault zones (Fig. 8a). For example, in the west of the Zhenghe–Dapu fault zone, the NW fault zones are boundaries that divide the distribution of Vp. Going to deeper depths (>12 km), low Vp and Vs values begin to appear beneath the Zhenghe–Dapu fault zone and can extend down to 39 km in depth (Fig. 8a and b). Beneath the Changle–Zhaoan fault zone, high Vp and Vs values begin to appear along the coastline (Fig. 8a and b). However, the map views of Vp/Vs ratios show low values at 0–12 km depths in most of the Fujian area, but, at deeper depths (>12 km), high values are distributed in most of the region, except those beneath the Zhenghe–Dapu fault zone. Notably higher values of Vp/Vs ratios are in southeastern Fujian along the coastline (Fig. 8c).

Figs. 9 and 10 show the EW and NS cross-sections, respectively, of Vp, Vs and Vp/Vs ratios. A widespread low Vp and Vs are at 10–20 km depths, and the lowest Vp is at the center of the Fujian (Profiles EW3 in Fig. 8b and d and NS2 in Fig. 10b and d). However, high Vp and Vs at 20–39 km depths can be observed along the coastline of Fujian beneath the Changle–Zhaoan fault zone (Figs. 9 and 10). On the other hand, low Vp/Vs ratios are distributed at 0–15 km depths and those low Vp/Vs ratios corresponding to low Vp ranges from 0 to 30 km depths beneath the Zhenghe–Dapu fault zone (Figs. 9c and 10c). The high Vp/Vs ratios with high Vp are distributed in the middle to lower crust near the coastline and rise to depths of approximately 10 km, as shown in Figs. 9c and 10c.

5. Discussion

Huang et al. (2010) and Zheng et al. (2013) used teleseismic events to invert the upper mantle structure and the crust and upper mantle structure beneath SE China, respectively. However, with their sources, the crustal structure at shallow depths is limited or cannot be resolved because most teleseismic rays traveled nearly vertical to the receivers (Zheng et al., 2013) or due to the crustal correction based on CRUST2.0 (global crust model; Bassin et al., 2000) fixed in the model (Huang et al., 2010). For comparison between these two models, in images at depths of 50–150 km, velocity perturbations show entirely different patterns in the Fujian area. The results of Huang et al. (2010) show a low dVp zone on land beneath the Zhenghe–Dapu fault zone but a high dVp zone beneath the Changle–Zhaoan fault zone along the coastline, while
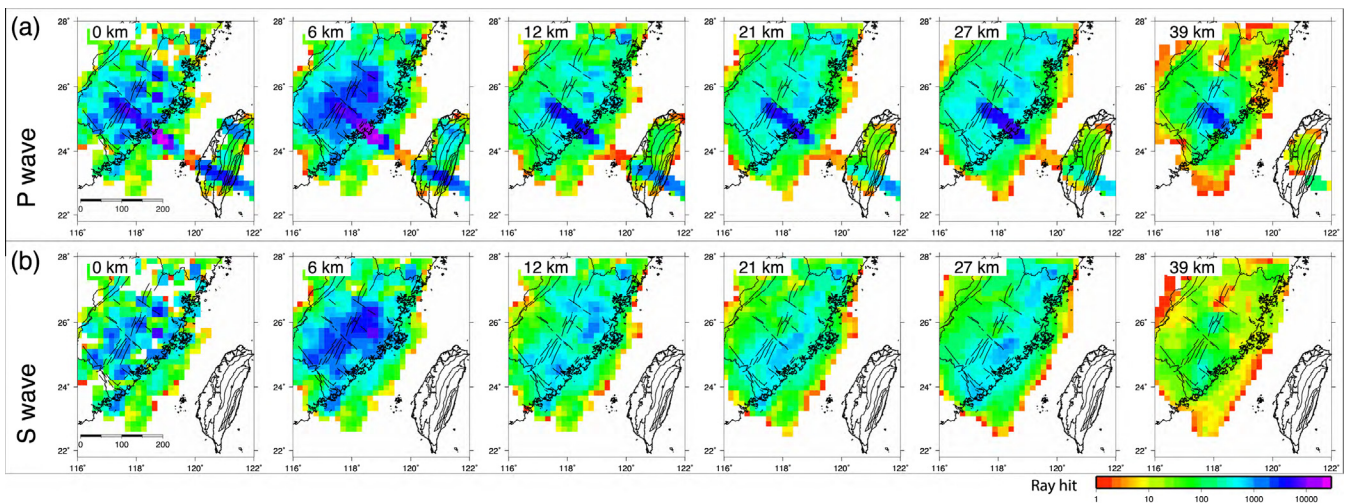

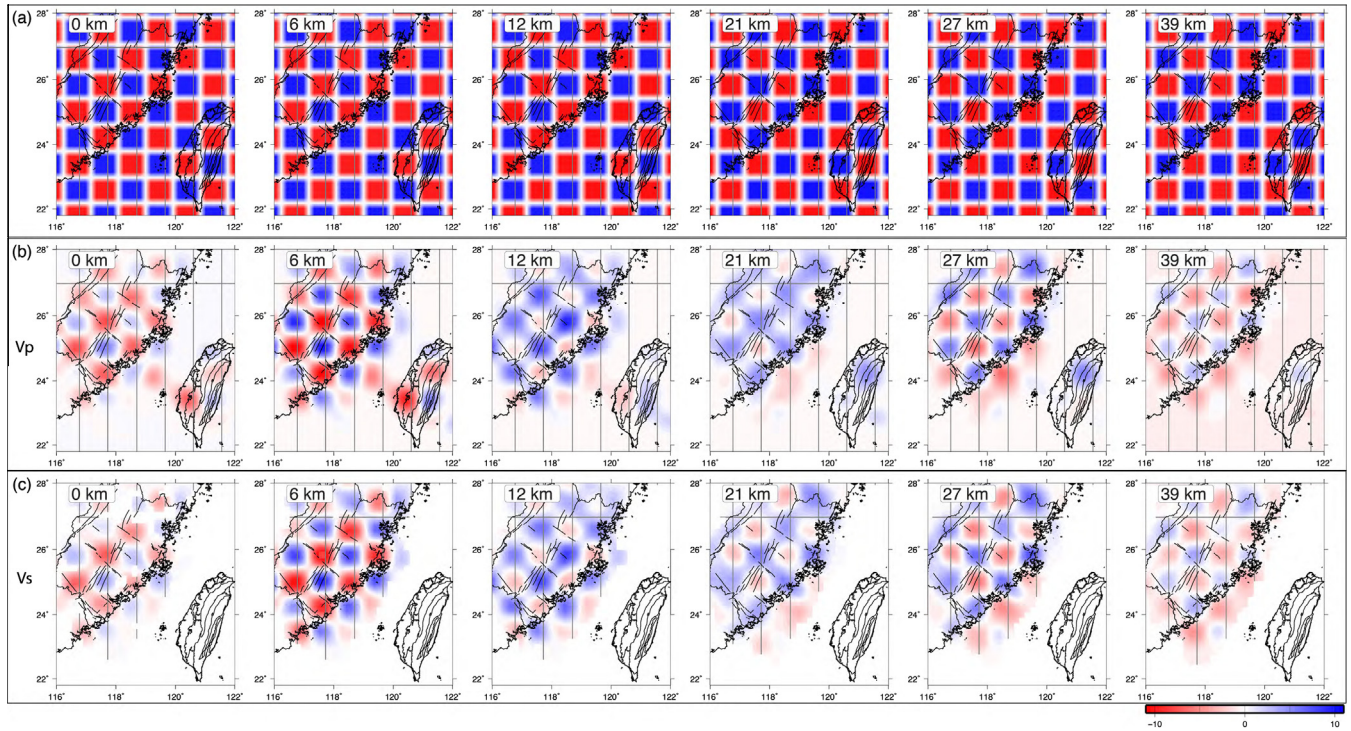**Fig. 6.** Numbers of ray hits at different depths. (a) P wave. (b) S wave.

Fig. 7. Checkerboard test at different depths. (a) Initial input checkerboard model. (b) Resolved checkerboard model of P waves. (c) Resolved checkerboard model of S waves.
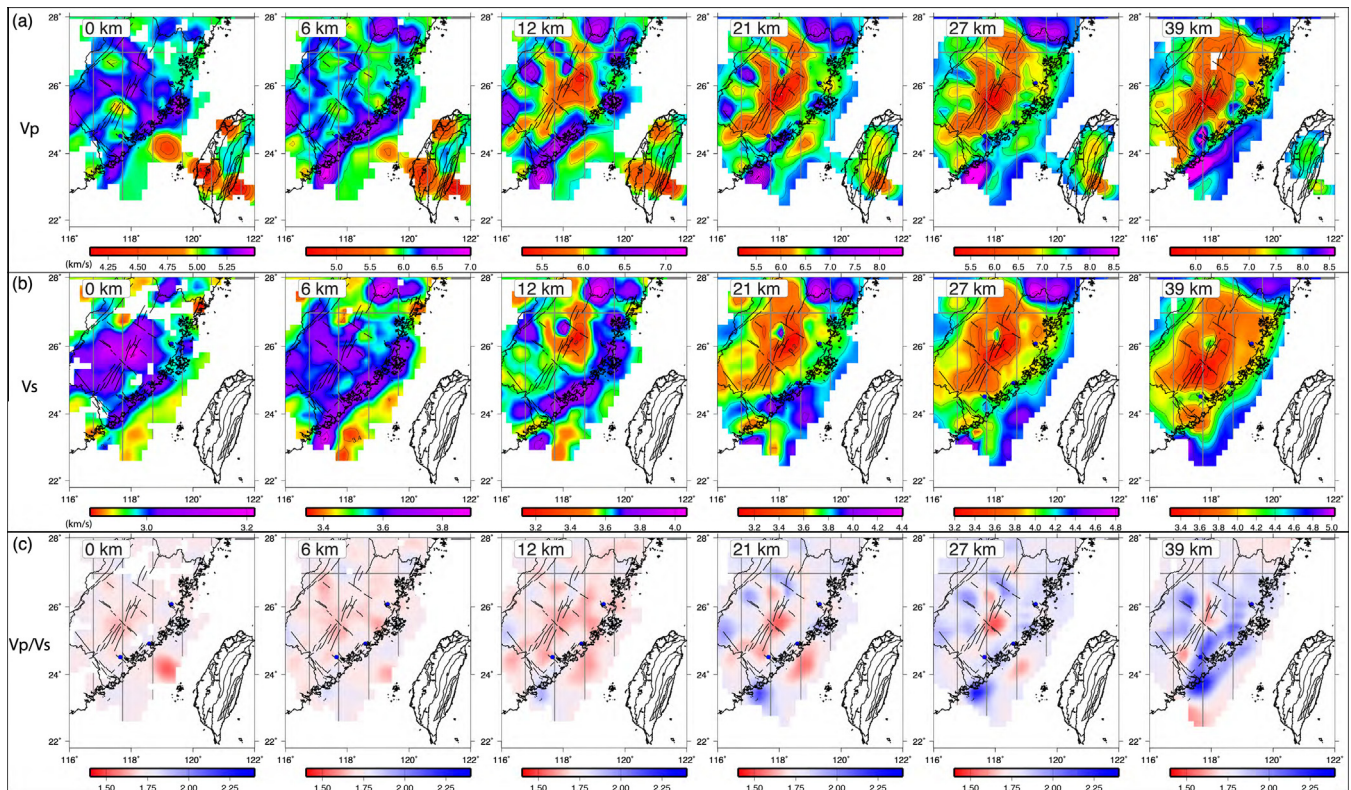

Fig. 8. Map view of (a) Vp, (b) Vs, and (c) Vp/Vs model at different depths.
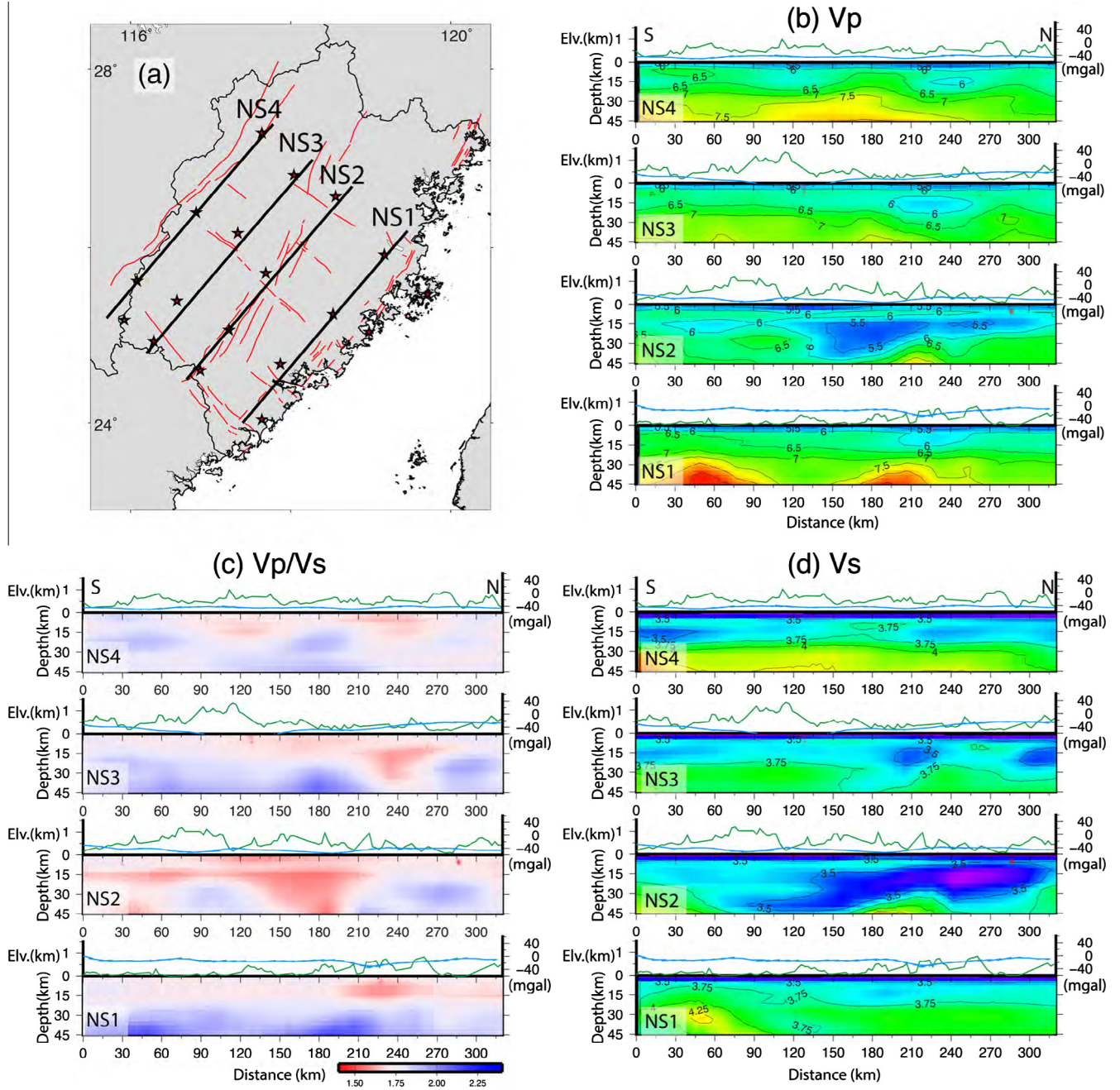
Fig. 9. EW vertical cross-sections of Vp, Vs, and Vp/Vs tomography. (a) Map view of cross-section locations. Red star: explosion. (b) EW cross-sections of Vp tomography. (c) EW cross-sections of Vp/Vs tomography. (d) EW cross-sections of Vs tomography. Green line: elevation. Blue line: Bouguer anomaly. Black arrow: coastline. (For interpretation of the references to color in this figure legend, the reader is referred to the web version of this article.)

the patterns in the results of Zheng et al. (2013) are reversed. The discrepancy between these two models is intriguing and must be explored further. Although we do not have the resolution of the upper mantle in this study, we can check the depths of the images, which are resolved among the models. There is no resolution at approximately 30 km depth in the work of Huang et al. (2010) because of the crustal correction applied to the tomographic inversion. Therefore, we compared the images at 45 km depth from this study with those at the similar depth of 50 km from Huang et al. (2010). As a result, the overall patterns of the images in Fujian are similar to each other but are more detailed in our results

(Fig. 11). It is worth mentioning that due to the 1D crustal correction of Huang et al. (2010), the velocity perturbations of the crust will be distributed at the top few layers of their model. In Figs. 8–11, the low-velocity zone is widely distributed beneath the Zhenghe–Dapu fault zone, which is a significant structure in Fujian, from Huang et al. (2010) and this study; thus, we performed another test for the resolution of this low-velocity zone. As a result, the pattern of this low-velocity zone can be resolved (Figs. 12 and 13). However, the results of Zheng et al. (2013) at the shallower depths of 10 and 25 km are opposite those of our study, and the images at deeper depths (50–150 km) as discussed above are also
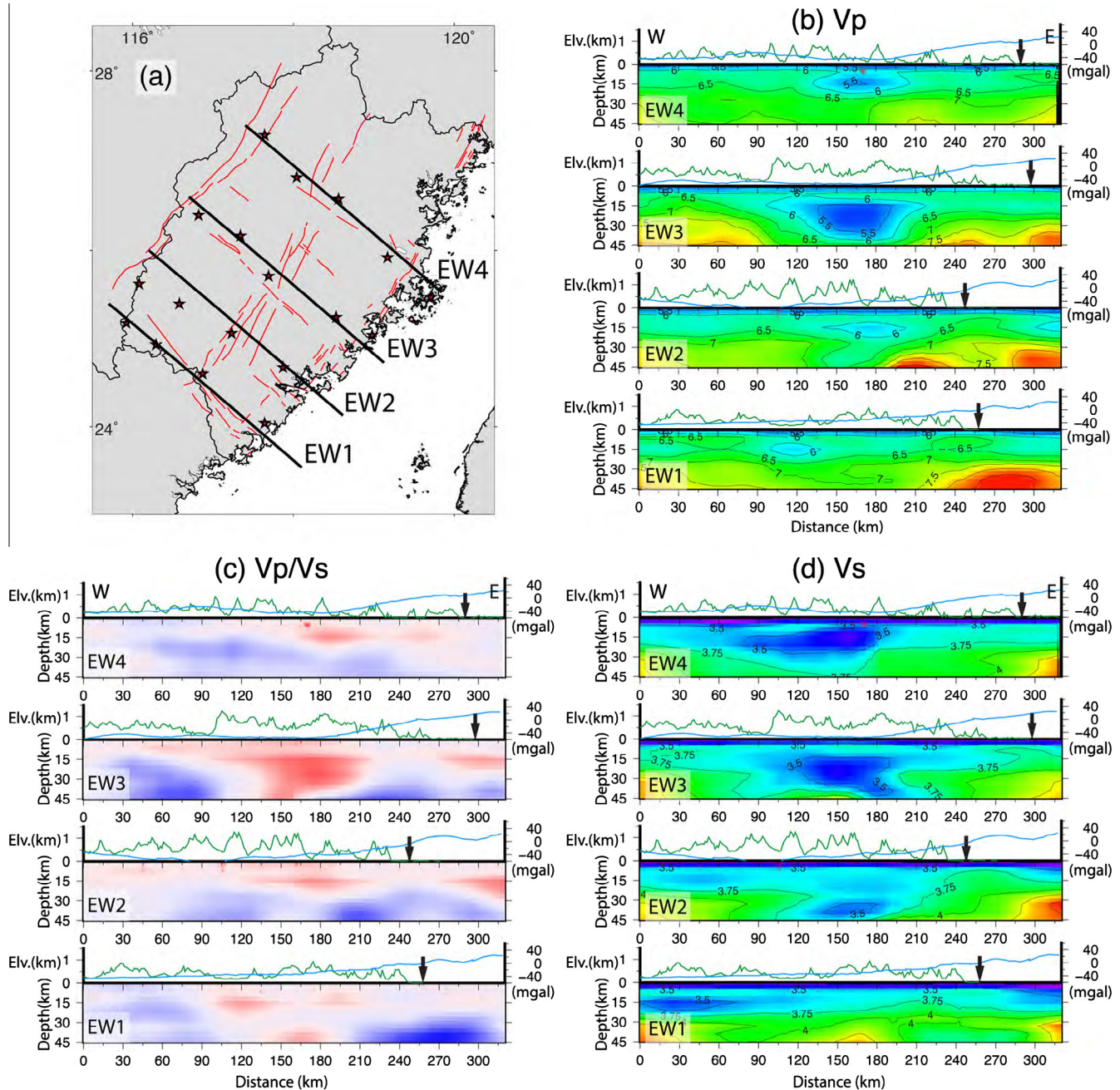
Fig. 10. NS vertical cross-sections of Vp, Vs, and Vp/Vs tomography. (a) Map view of cross-section locations. Red star: explosion. (b) NS cross-sections of Vp tomography. (c) NS cross-sections of Vp/Vs tomography. (d) NS cross-sections of Vs tomography. Green line: elevation. Blue line: Bouguer anomaly. Black arrow: coastline. (For interpretation of the references to color in this figure legend, the reader is referred to the web version of this article.)

opposite those of Huang et al. (2010); the discrepancy of the images between Zheng et al. (2013) and others is not easily explained.

Laboratory measurements show that Vp/Vs ratios are sensitive to rock compositions, but Vp or Vs alone is insufficient for separating them from pressure and temperature effects (Kern, 1982). The information of P wave velocity incorporated with Vp/Vs ratio can assist in distinguishing the rock compositions (Kern, 1982; Christensen and Mooney, 1995; Christensen, 1996). Hence, laboratory Vp/Vs ratios of rocks have been used to interpret seismic velocity ratios in terms of crustal rock materials. Vp/Vs ratios for

crack-free rocks vary in the range of 1.5–1.9, with quartz-rich rocks generally in the lower and mafic rocks in the higher ranges (Christensen, 1996).

At the surface of Fujian, most rocks are quartz-rich, composed of magmatic granitoid of the Pre-Cambrian and Cambrian Eras, granite of the Mesozoic, and sedimentary rocks of the Paleozoic and Mesozoic (Fujian, 1985). The 3D distribution of quartz-rich rocks can be identified in terms of lower Vp/Vs ratios as described above. At the surface, the Vp/Vs ratios in most of the area are in the lower range (~1.6–1.7), which is consistent with geological observations, except those values along the coastline with the higher range
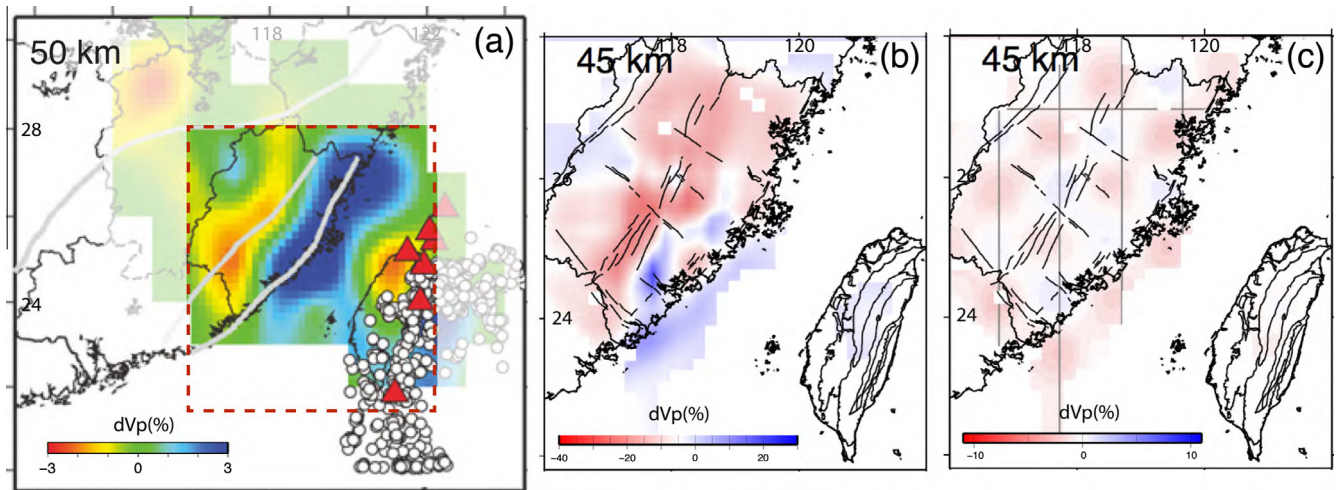
Fig. 11. Comparison with the tomography of Huang et al. (2010) at 50 km depth. (a) Tomography of Huang et al. (2010) at 50 km depth. White circle: earthquake. Red triangle: seismic station. Gray line: fault zone. (b) dVp tomography at 45 km depth in this study. (c) Resolved checkerboard test of Vp tomography at 45 km depth in this study. (For interpretation of the references to color in this figure legend, the reader is referred to the web version of this article.)
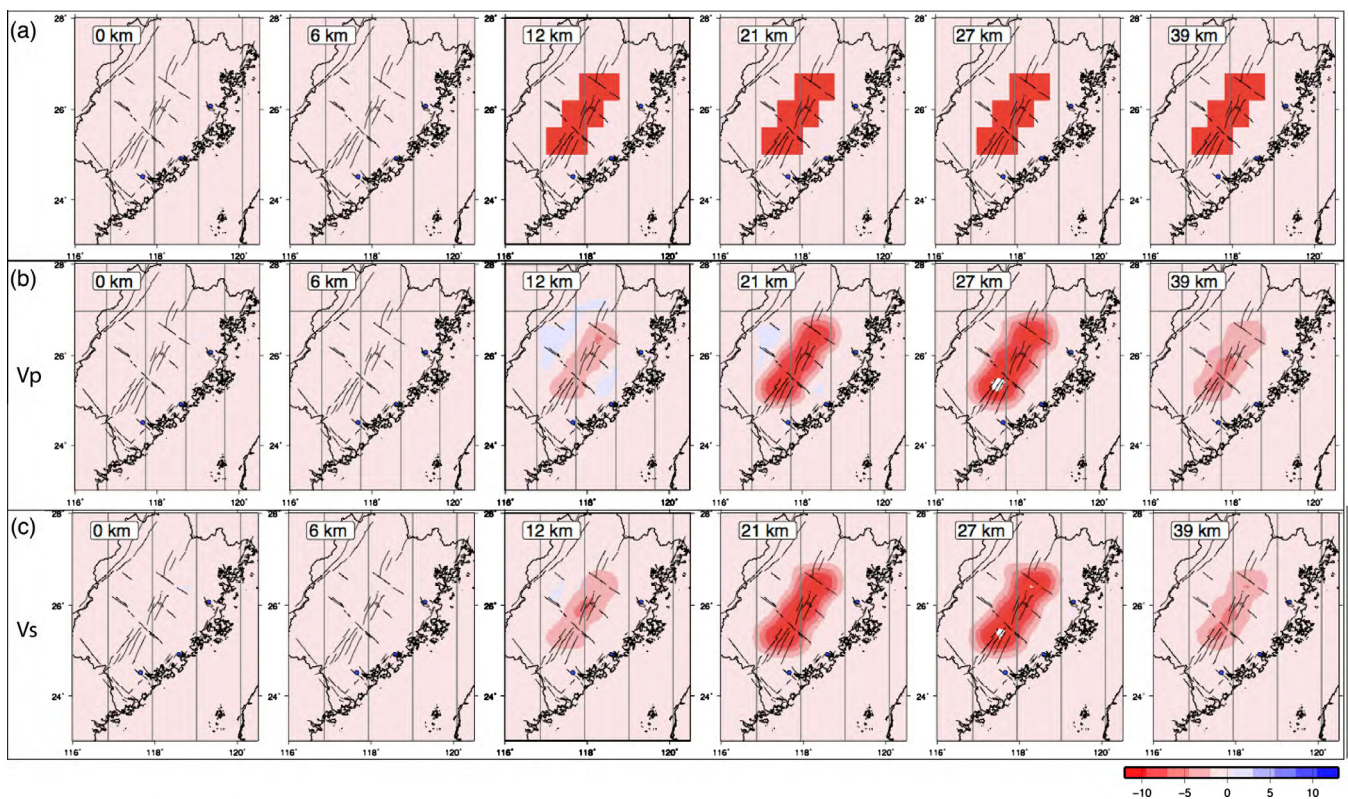

Fig. 12. Resolution test of the low-velocity zone in the center of Fujian. (a) Map view of the initial model at different depths. (b) Map view of the resolved model of Vp tomography. (c) Map view of the resolved model of Vs tomography.

(Figs. 9 and 10). The high values of Vp/Vs ratios could be related to the hot springs along the coastline at shallow depths (Fujian, 1992) and will be discussed below. At deeper depths, the distribution of the lower Vp/Vs ratios is centered in the Zhenghe–Dapu fault zone down to 30 km depth and even to deeper depths in the southern part of the Zhenghe–Dapu fault zone (Figs. 9 and 10), which could

indicate that the crust of the Fujian is mainly composed of felsic rocks as part of the Eurasian continental crust. However, the anomalously high Vp/Vs ratios and Vp distributed along the coast-line beneath the Changle–Zhaoan fault zone can be observed at all depths (Figs. 9 and 10) and correspond with high heat flows. As no upwelling features are observed in the mantle beneath this region
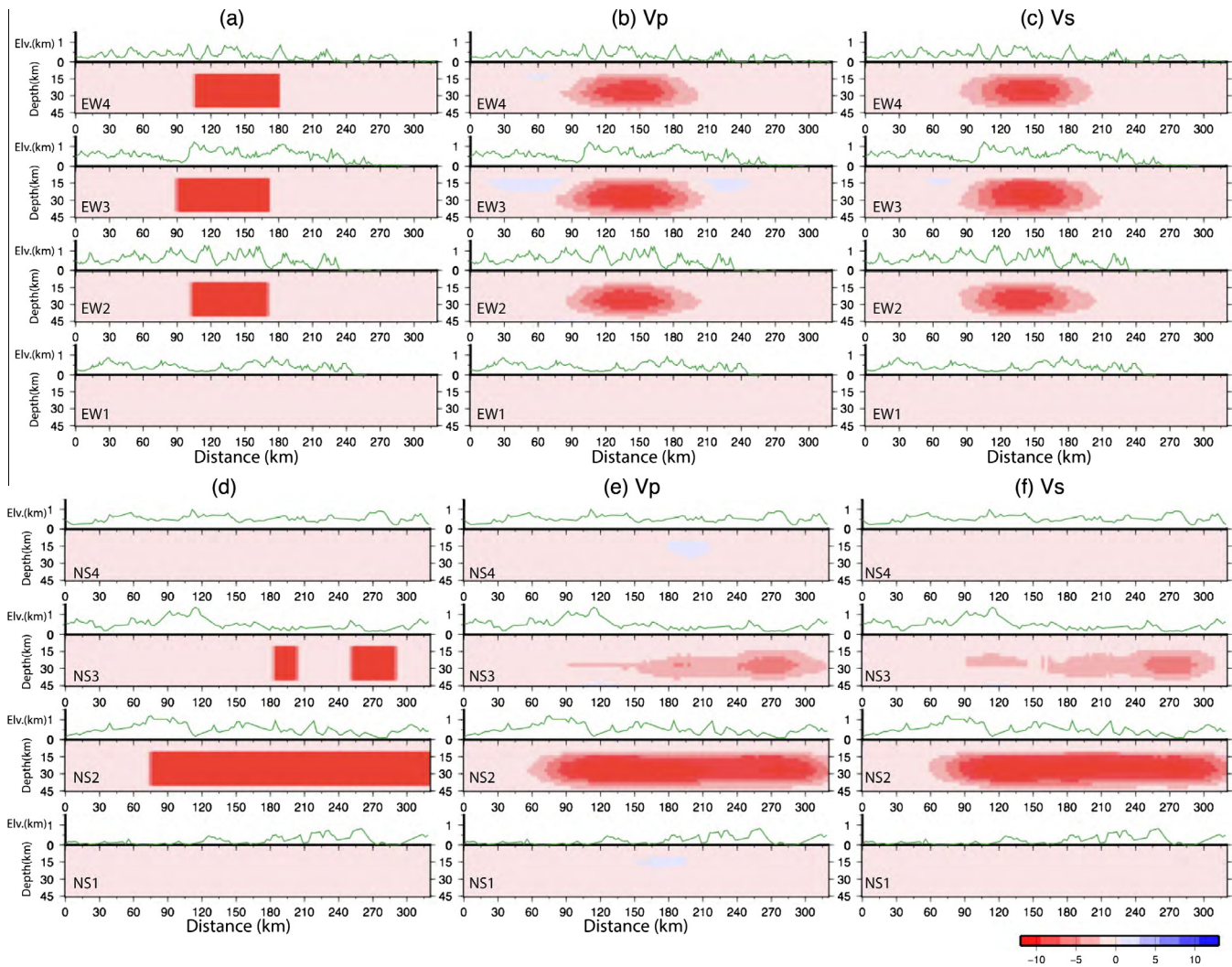
Fig. 13. Resolution test of the low-velocity zone in the center of Fujian. (a) EW cross-sections of Fig. 8 of the initial model at different depths. (b) Resolved model of the EW cross-sections of Vp tomography. (c) Resolved model of the EW cross-sections of Vs tomography. (d) NS cross-sections of Fig. 9 of the initial model. (e) Resolved model of the NS cross-sections of Vp tomography. (f) Resolved model of the NS cross-sections of Vs tomography.

from regional tomography (Huang et al., 2010), we interpret this shallow crust phenomenon could be related to the regional extensional stress. There are two possibilities during the multi-stage tectonic evolution in Fujian: (1) the remaining structure of the back-arc extension that stretched the continental crust in the Mesozoic Era (e.g., Jahn et al., 1976; Chen et al., 2002; Wang and Shu, 2012); or (2) the Cenozoic extension due to South China sea opening in Taiwan Strait (Li, 2013).

In general, the locations of earthquakes in Fujian were above 30 km depth, and seismicity was relatively high offshore of southeastern Fujian and in the southern part of the Zhenghe–Dapu fault zone (Fig. 14). The locations of historical large earthquakes are related to those active seismogenic zones (Fig. 1b). However, the mechanisms of active fault zones are important to provide information of the current stress and should be studied further. The depth variation of earthquakes across Fujian is an indicator for the geothermal distribution of the crust. In Fig. 13, we show the NS profiles from west to east and calculate the earthquake occurrence at different depths. Most earthquakes occurred above 10 km depth, and, in the central profiles (Fig. 14) near the Zhenghe–Dapu fault zone, some earthquakes occurred below 10 km depth, which implies that the geothermal gradient is

relatively low in the center of Fujian (Zhenghe–Dapu fault zone) and increases toward the east and west. These observations are consistent with the distribution of heat flow data (Fujian, 1992).

6. Conclusion

Based on historical earthquake records, the seismic hazard risk in Fujian and its offshore is potentially high, and seismicity in this study has also indicated that the local seismogenic zones, the Zhenghe–Dapu and Changle–Zhaoan fault zones, are very active. The 3D Vp, Vs, and Vp/Vs crustal structures have shown that the rock compositions of the crust are quartz-rich in most of the Fujian area, except along the coastline. Along the coastline, the thickness of the crust is shallower than that on land, which is related to the higher heat flow and Bouguer anomaly.
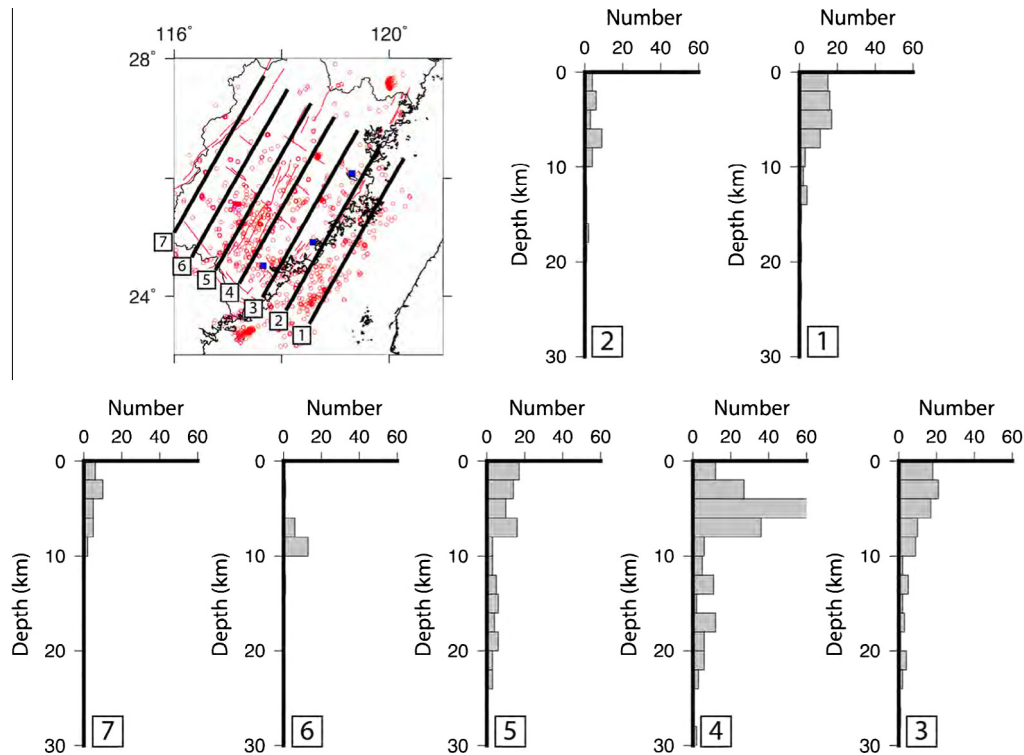
Fig. 14. Depth histograms of seismicity in NS cross-sections. (Left upper panel) Map view of cross-section locations. Red circle: earthquake after 3D velocity model relocation. Histogram with number: depth distribution of seismicity along the corresponding number of the cross section in map view (seismicity within 10 km width on both sides of the central line of the cross-section is selected). (For interpretation of the references to color in this figure legend, the reader is referred to the web version of this article.)

References

Bassin, C., Laske, G., Masters, G., 2000. The current limits of resolution for surface wave tomography in North America. EOS Trans. AGU 81, F897.

Cai, H.-T., Jin, X., Wang, S.-X., 2015. The 1-D crust velocity structure in the continental margin of Southeast China. Terr. Atmos. Ocean. Sci. http://dx.doi.org/10.3319/TAO.2015.04.08.01(T).

Chen, W.S., Yang, H.C., Wang, X., Huang, H., 2002. Tectonic setting and exhumation history of the Pingtan–Dongshan metamorphic belt along the coastal area, Fujian Province, southeast China. J. Asian Earth Sci. 20, 829–840.

Christensen, N.I., Mooney, W.D., 1995. Seismic velocity structure and composition of the continental crust: a global view. J. Geophys. Res. 100, 9761–9788.

Christensen, N.I., 1996. Poisson's ratio and crustal seismology. J. Geophys. Res. 114, 3139–3156.

Ding, X.H., Wang, Y.D., Ye, S.J., 1999. Active Faults and Earthquakes in Southeastern Coast of Fujian. Fujian Science and Technology Publishing, p. 223 (in Chinese).

Fujian (Bureau of Geology and Mineral Resources of Fujian Province), 1985. Regional Geology of Fujian Province. Geological Publishing House (in Chinese with English Abstract).

Fujian (Bureau of Geology and Mineral Resources of Fujian Province), 1992. Geophysical Investigations of the Geothermal Resources in Fujian Province, 273.

Hole, J.A., Zelt, B.C., 1995. 3-D finite-difference reflection traveltimes. Geophys. J. Int. 121, 2427–2434.

Hu, S.B., He, L.J., Wang, J.Y., 2000. Heat flow in the continental area of China: a new data set. Earth Planet. Sci. Lett. 179 (2), 407–419.

Huang, J., Zhao, D., 2006. High-resolution mantle tomography of China and surrounding regions. J. Geophys. Res. 111, B09305. http://dx.doi.org/10.1029/2005JB004066.

Huang, Z., Wang, L., Zhao, D., Xu, M., Mi, N., Yu, D., Li, H., Li, C., 2010. Upper mantle structure and dynamics beneath Southeast China. Phys. Earth Planet. Inter. 182, 161–169.

Jahn, B.M., Chen, P.Y., Yen, T.P., 1976. Rb-Sr ages of granitic rocks in southeastern China and their tectonic significance. Bull. Seismol. Soc. Am. 86, 763–776.

Kern, H., 1982. Elastic-wave velocity in crustal and mantle rocks at high pressure and temperature: the role of the high-low quartz transition and of dehydration reactions. Phys. Earth Planet. Inter. 29, 12–23.

Li, X., 2013. Subdivision and characteristic of tectonic units in Fujian Province. Global Geol. 32, 549–557 (in Chinese with English abstract).

Roecker, S., Thurber, C., McPhees, D., 2004. Joint inversion of gravity and arrival time data from Parkfield: new constraints on structure and hypocenter locations near the SAFOD drill site. Geophys. Res. Lett. 31, L12S04. http://dx.doi.org/10.1029/2003GL019396.

Roecker, S., Thurber, C., Roberts, K., 2006. Refining the image of the San Andreas Fault near Parkfield, California using a finite difference travel time computation technique. Tectonophysics 426, 189–205.

Shu, L.S., Faure, M., Yu, J., Jahn, B.-M., 2011. Geochronological and geochemical features of the Cathaysia block (South China): new evidence for the Neoproterozoic breakup of Rodinia. Precambr. Res. 187 (3–4), 263–276.

Vidale, J.E., 1988. Finite-difference calculation of travel times. Bull. Seismol. Soc. Am. 78, 2062–2076.

Wan, T.F., 2012. The Tectonics of China: Data, Maps and Evolution. Higher Education Press and Springer, Beijing, Heidelberg, Dordrecht, London, New York, p. 501.

Wang, D., Shu, L., 2012. Late Mesozoic basin and range tectonics and related magmatism in Southeast China. Geosci. Front. http://dx.doi.org/10.1016/j.gsf.2011.11.007.

Wu, F.T., Kuo-Chen, H., McIntosh, K., 2014. Subsurface imaging, TAIGER experiments and tectonic models of Taiwan. J. Asian Earth Sci. 90, 173–208.

Yu, S.B., Chen, H.Y., Kuo, L.C., 1997. Velocity of GPS stations in the Taiwan area. Tectonophysics 274, 41–59. http://dx.doi.org/10.1016/S0040-1951 (96)00297-1.

Zheng, H.W., Gao, R., Li, T.D., Li, Q.S., He, R.Z., 2013. Collisional tectonics between the Eurasian and Philippine Sea plates from tomography evidences in Southeast China. Tectonophysics 606, 14–23.